JOURNAL OF GUIDANCE, CONTROL, AND DYNAMICS
Vol. 29, No. 2, March–April 2006

Full-Envelope Robust Control of a Shrouded-Fan Unmanned Vehicle

Giulio Avanzini*
Politecnico di Torino, 10129 Turin, Italy
Umberto Ciniglio†
Italian Aerospace Research Center, 81043 Capua, Italy
and
Guido de Matteis‡
University of Rome "La Sapienza," 00184 Rome, Italy

The development is described of a rate-command system for the control of a novel unmanned vehicle, the baseline model of which is highly nonlinear and presents fast and unstable open-loop modes. Structured singular-value design methodology is used to achieve the desired command response characteristics under specified uncertainties taking into consideration typical problems of small-size helicopters and ducted-fan vehicles such as rate-limited servos and significant time delays. Two robust linear controllers are designed for the low- and high-speed subsets of the operating envelope, and full-envelope flight control is achieved by switching between controllers as the threshold airspeed is traversed. Following an analysis of scaling effects, controller performance is evaluated against rotorcraft handling-qualities specifications. Flight control system development is assessed by piloted, hardware-in-the-loop simulation in the full range of operating conditions, with the controller implemented in the flight computer and pilot commands transmitted to the vehicle via radio link. Simulation testing also shows that the control system has good turbulence gust rejection performance and is robust to significant variations of c.g. position.

Nomenclature

$\boldsymbol{a}$	=	actuator angle vector
$\bar{\boldsymbol{a}}$	=	actuator activity
$\bar{\boldsymbol{e}}$	=	performance error
F_u, F_l	=	upper and lower fractional transformation, respectively
h	=	altitude
$\boldsymbol{I}$	=	unit matrix
$\boldsymbol{K}$	=	controller
$\boldsymbol{K}_{\mathrm{PI}}$	=	proportional-integral element
$\boldsymbol{n}$	=	noise
p, q, r	=	roll, pitch, and yaw rate
R	=	rotor radius
$\boldsymbol{r}$	=	command
$\bar{\boldsymbol{r}}$	=	reference signal
s	=	Laplace variable
u, v, w	=	velocity components in body frame
$\boldsymbol{u}_s$	=	input to servos
$\bar{\boldsymbol{u}}$	=	controller output
V	=	airspeed
$\boldsymbol{w}$	=	perturbation
$\boldsymbol{x}$	=	state vector
$\boldsymbol{y}$	=	output to controller
$\boldsymbol{z}$	=	uncertainty
δ_A, δ_B	=	lateral and longitudinal cyclic input
δ_C	=	collective control input
δ_P	=	differential collective
ϑ	=	blade pitch angle
μ	=	structured singular value
ϕ, θ, ψ	=	roll, pitch and yaw angle
ψ_b	=	blade azimuth angle

Subscripts

com	=	command
H	=	at hovering
HS, LS	=	high and low speed
hg	=	high gain
U, L	=	upper and lower rotor
$\| \|_\infty$	=	infinity norm

Presented as Paper 2003-5521 at the AIAA Guidance, Navigation, and Control Conference, Austin, TX, 11–14 August 2003; received 29 October 2004; revision received 20 April 2005; accepted for publication 20 April 2005.

*Assistant Professor, Department of Aerospace Engineering, C. so Duca degli Abruzzi, 24. Member AIAA.
†Senior Researcher, Department of Flight Systems, Via Maiorise.
‡Professor, Department of Mechanics and Aeronautics, Via Eudossiana, 18. Member AIAA.

I. Introduction

A ROBUST full-envelope flight control system (FCS) for a shrouded-fan uninhabited aerial vehicle (UAV) is developed. The structured singular value μ synthesis is used to address most of the key challenges experienced in FCS design and implementation for this class of unconventional UAVs and, in general, for small-size rotorcraft. To account for the large variation of plant dynamics in the range of operating conditions, two controllers are switched as the vehicle flies across the design points. Validation of FCS is conducted by pilot-in-the-loop flight simulation in a dedicated facility.

The tilting-type UAV, where forward flight is realized by thrust vector deflection, has a maximum takeoff weight of 900 N and is powered by three two-strokes, air-cooled engines each rated at 14 hp at 11,000 rpm. Two counter-rotating, three-bladed rotors of 0.5 m radius, operating at an angular speed of 3000 rpm are shrouded by a doughnut-shaped airframe the external diameter of which is 1.8 m. The design, shown in Fig. 1, is presented in detail in Refs. 1 and 2.

The vehicle uses collective and cyclic blade-pitch variation to control thrust force and moment generated by the rigid, not flapping rotors. Two independent swashplates provide blade-pitch control by means of a set of six dual servos commanded by four channels for collective pitch, longitudinal and lateral cyclic pitch, and differential collective. The latter is used to unbalance total rotor torque so as

Fig. 1 Perspective view of the UAV solid model.

Fig. 2 UAV prototype.

to generate yaw control moments.[1] Ground pilot control is realized through a right-hand, three-axis joystick for pitch, roll, and yaw commands, and a left-hand lever for vertical velocity control. The UAV prototype, shown in Fig. 2, is currently in the final phase of development after completion of flawless ground tests for rotor, engine, and avionic systems, and constrained flight testing is being planned as the next step.

Among ducted-fan vertical-takeoff-and-landing (VTOL) vehicles, the design shares some analogies with the Sykorsky Cypher,[3] where two coaxial bearingless rotors are driven by a Wankel-type rotary engine located in the shroud. On the converse, differences are quite significant in terms of size and configuration with respect to the Micro Craft iSTAR microair vehicles (MAV)[4] that use a fixed-pitch propeller for thrust generation while attitude control is realized by actuated vanes.

Control system design for robotic and/or remotely piloted rotorcraft has been carried out extensively in recent years using a variety of methods from classical control[4] to neural-based adaptive control.[5] Small-scale radio-controlled (RC) rotorcraft represent fairly demanding applications for control synthesis because of issues such as poor modeling, high rotor speed (1000–1500 rpm) and rate and bandwidth-limited servos. Usually, miniature helicopters, as for instance the X-Cell.60 and the Yamaha agricultural vehicles R-50 and RMAX used for UAV research,[6–8] have a Bell–Hiller stabilizer bar acting as a lagged-rate feedback system to introduce damping on the fast attitude dynamics, and present marginally stable or unstable translational dynamics at low speed with time constant of tens of seconds.[6]

The influence of physical scale on performance characteristics and flying qualities of miniature rotorcraft is investigated in Refs. 9 and 10. Scaling laws, based on a relatively small set of physical parameters, are derived to classify the agility of a given rotorcraft and, in turn, to provide design guidelines where suitability of the class of vehicle for the envisioned application is taken into consideration. It is demonstrated that stringent bandwidth requirements on hardware (HW) components result from the overall faster dynamics of small-scale rotorcraft.[10]

The dynamic characteristics of the UAV addressed in this study, evaluated for a model based on a preliminary design of the shroud, are described in detail in Ref. 1. In short, the open-loop dynamics presents a dominant unstable response in pitch as a result of the large variation of aerodynamic pitching moment over the airspeed envelope, which is also a primary source of aerodynamic uncertainty. The large value of the pitching-moment derivative, typical of ducted-fan configurations,[1,3] makes the vehicle highly sensitive to winds and turbulence. Additional uncertainty results from the complexity inherent in the aerodynamic system because of the interference between rotor and shroud flow,[1] and the approach adopted for the generation/validation of the vehicle model where the analysis of flowfield, carried out by numerical methods, is not supported by wind-tunnel or whirl-tower tests.

In comparison with the aforementioned RC helicopters, inertia is of the same order of magnitude as in the Yamaha R-50 while rotor rpm is much higher, and the unstable pendulum dynamics have time constants as low as 2 s at hovering because of the short vertical distance between c.g. and rotor center.[1] Frequency separation between translational and attitude modes is therefore small, such that it would be difficult to treat the two sets of dynamics independently or sequentially in FCS design. Further control problems, common to miniature rotorcraft and ducted-fan vehicles, are actuator rate/position limits, significant delays associated with servo dynamics and control HW (CPU, sensors, filters), and sensor vibration and drift.

Unlike helicopters, the axial symmetry of the shroud limits the coupling between responses to longitudinal and lateral control inputs, but it is also the cause of practically negligible directional stability and yaw damping, resulting from the absence of stabilizing surfaces. Moreover, some level of interference in the response to vertical and directional commands is as a result of the servo arrangement because the gear ratios in the upper and lower rotor linkages are different. This problem is only partially alleviated by the introduction of interlinks between servo input signals to minimize coupling resulting from pilot commands.

The control problem in ducted-fan configurations is basically to provide attitude stabilization to highly unstable systems that present significant variations in vehicle dynamics. Attitude control systems realized by the closure of classical single-input/single-output (SISO) loops were successfully flight tested for a range of vehicle sizes,[4] whereas a sliding multiple mode multiple-input/multiple-output controller[11] was shown to exhibit stability and performance robustness superior to that of a classical SISO design.

The main contribution of this paper is the definition of a control design approach and the evaluation of a suitable solution for an original VTOL configuration, where the typical, and aforementioned, control issues of a category of small-size, rotary wing UAVs are addressed in detail. Accordingly, the major design objective is to realize robust controllers that can operate with limited degradation of tracking performance in a wide airspeed range about the nominal condition, thus avoiding the necessity of gain scheduled outer-loop designs. The μ-synthesis method[12] is used because, in comparison with other variants of H_∞-based methods, the calculated controller achieves the prescribed performance specifications under the considered uncertainty structure. Also relevant in the selection of the μ-synthesis process was the fact that it accounts for the low bandwidth of servos, realistic levels of time delay in the system, and high- and low-frequency modeling uncertainties caused, respectively, by neglected rotor/engine dynamics and plant nonlinearities together with poor aerodynamic modeling.

Robust control based on H_∞ and structured singular value[12] design methodology has been extensively used in robotic rotorcraft FCS design.[13] Unlike the case of H_∞ loop shaping,[14] in which controller structure is fixed if the frequency-dependent weights used to shape the plant have identical structure, the technique produces dynamic controllers, the structure of which is not, in general, defined, and the synthesis of a full-envelope FCS by individual point designs and gain scheduling is a major problem. Conversely, a small set of controllers can be defined, each covering a large subset of the operating envelope, so that control activity is switched between them as the vehicle flies across the boundaries of specified operating regions.[15]

In Ref. 16 a two-level approach was adopted, in which robust stability and uncoupled response are provided by a four-axis inner multivariable loop using rates p, q, r, and vertical velocity $\dot{h}$, whereas outer SISO loops realize the desired attitude-command attitude-hold response type. Controller evaluation by μ analysis showed acceptable levels of robust stability. However, the inner-/outer-loop design had some drawbacks, that is, 1) an unwanted coupling between yaw and heave axes following heave velocity inputs at the inner level, which is only partially solved by the outer loops for attitude hold; 2) an inherent complication in satisfying handling-qualities requirements because it is difficult to explicitly include in the design process the coupling between inner and outer control loops; and 3) a poor level of robust performance. This aspect is somewhat complicated by the fact that the SISO loop gains would require scheduling to account for the significant uncertainty of the nominal plant at flight speeds different from the design point.

To address and possibly solve the aforementioned problems, the synthesis of a new controller is undertaken, which, in principle, shares some features of the original design such as the two-degrees-of-freedom (DOF) structure,[17,18] the fact that the dynamic characteristics of the servos are taken into consideration in the synthesis model of the platform and, finally, the use of μ-design technique. The two-DOF architecture, where reference and feedback signals (angular rates and heave velocity) are separate inputs in order to decouple the properties of the feedback loop (i.e., robustness) from those of closed-loop command following, is less sensitive to disturbances and model uncertainty.[19]

A rate-command control system, where angular velocities about body axes proportional to command inputs are generated, is considered more suitable for remotely piloted operations. Rate-command attitude-hold (RCAH) response type is realized by shaping the plant with a filter with proportional-plus-integral (PI) action on the command input channels. Provided that the issue of the integrator pole at the origin not handled by μ analysis is addressed through an appropriate definition of the weight on control activity, the PI element allows the μ controller to be designed as a whole without entailing the more classic architecture based on an inner/outer structure. According to the envisioned single-loop control and RC ideal step response model, precise AH response cannot be achieved in the presence of random disturbances at plant input. This is a minor problem, as we assume that a slow drift of attitude angles during flight in turbulence can be easily controlled by ground operator commands or autopilot loops.

Two linear controllers for the low- and high-speed subsets of the operating envelope are designed, and smooth transition of actuator commands during switching is obtained through the so-called high gain approach.[15] Of course, relaxed requirements on transient motion during switching, in comparison with manned vehicles, can be acceptable for a remotely piloted vehicle.

Although important in principle, scaling of the handling-qualities requirements is not easily applicable for the proposed rotorcraft. As stated in Ref. 10, in which Froude scaling is applied to a model helicopter, an approach based on similarity requires that vehicles of different sizes share the main features of their configuration. In this respect, the shrouded-fan configuration is considerably different from a conventional helicopter in terms of both aerodynamics and mass distribution, and this fact has immediate consequences on the scaled configuration coefficients, when rotor radius is used as the representative length in the scaling procedure. This concept is demonstrated in Table 1, in which the comparison discussed in Ref. 9 between the Yamaha R-50 model helicopter and the UH-1H full-size vehicle is extended to include ducted-fan vehicles, such as the MicroCraft iSTAR[4] and the Sikorsky Cypher.[3] With respect to that study,[9] the parameters related to blade flapping are not included, inasmuch as they are not defined for the rigid rotors or propellers of most ducted-fan UAVs. The rotor radius of our UAV is used as the reference length R_0 for determining the scale factor $N = R/R_0$. Three columns are associated with each vehicle. The first one (labeled Data) indicates the actual value of the considered coefficients or geometric characteristics, the second column (Scaled) reports the corresponding scaled value (that is, the value obtained scaling the actual number according to the similarity law reported in the second column of the table), whereas the third one (Ratio) shows the ratio between the scaled parameter and the corresponding value for our vehicle. When the ratio is close to 1, the similarity is applicable and the smaller vehicle can be considered as a scaled version of the larger one.

It is apparent that the Sikorsky Cypher[3] and the present rotorcraft have similar values for all of the considered parameters, whereas the scaled data of both miniature and full-size helicopters are largely different from the data of our design. In particular, the ratios between scaled coefficients are considerably far from unity, with rotor solidity and scaled vehicle weight being of a different order of magnitude. Note also that the physical interpretation of Froude scaling for the iSTAR MAV[4] is far from trivial as, for this vehicle, 1) the two-bladed propeller has a much lower solidity than the aforementioned configurations featuring counter-rotating rotors and 2) high-speed forward flight is accomplished in a nearly horizontal attitude.

Evaluation of closed-loop performance of the UAV is therefore carried out against the ADS-33E specifications for full-scale military helicopters,[20] basically using the requirements as a reference for the assessment of handling qualities rather than as design criteria. The latter would require more fundamental questions to be addressed, concerning the effect of transport delays in telemetry, type of display used, and possibly ground operator modeling on attainable phase margins for ADS 33E compliance.

To assess command response characteristics, analyze robust performance under external disturbances and parameter uncertainty, and to evaluate vehicle handling qualities in a realistic scenario, flight simulations of the closed-loop system are conducted in a operator/pilot-in-the-loop simulation facility.[21] The hardware/software (HW/SW) components of the systems are a detailed nonlinear model of the vehicle running in real time, the ground control station, and the flight computer. The latter is connected by radio link to the ground station.

Table 1 UAV data scaling and comparison for $N = R/R_0$

Parameter	Scaling law	Our UAV data	UH-1H			R-50			Cypher			iSTAR MAV		
			Data	Scaled	(Ratio)	Data	Scaled	(Ratio)	Data	Scaled	(Ratio)	Data	Scaled	(Ratio)
Scaling factor N	——	1	14.63	——	——	3.07	——	——	1.22	——	——	0.23	——	——
Rotor radius B, ft	$1/N$	1.64	24.0	1.64	(1.00)	5.04	1.64	(1.00)	2.00	1.64	(1.00)	0.375	1.64	(1.00)
Solidity σ	1	0.30	0.046	0.046	(6.52)	0.05	0.05	(6.00)	0.30[a]	0.30	(1.00)	0.12	0.12	(2.50)
Weight W, lb	$1/N^3$	180	8000	2.55	(70.52)	150	5.17	(34.83)	300	165.41	(1.09)	4	334.58	(0.54)
Rotor speed Ω, rad/s	$\sqrt{N}$	314	34	130	(2.41)	89	156	(2.01)	300	331.3	(0.95)	1780	851.2	(0.37)
Norm. thrust coeff. C_T/σ	1	0.113	0.061	0.061	(1.86)	0.079	0.079	(1.43)	0.093	0.093	(1.21)	0.071	0.071	(.159)

[a]Parameter not available in the literature, estimated from vehicle drawings.

In what follows, after a brief presentation of UAV model dynamic characteristics, the design procedure is outlined in Sec. II, whereas the control system performance is evaluated and discussed in detail in Sec. III. A section of conclusions ends the paper.

II. Control Law Design

A. Vehicle Dynamics

Fast and unstable open-loop modes together with significant uncertainty and variation of parameters as function of flight speed represent the principal unfavorable dynamic characteristics of the UAV model.[1] The root locus of the linear model vs trim speed in the full range of level flight conditions ($0 \le V \le 30$ m s^{-1}) reported in Fig. 3 shows that two divergent oscillatory modes, namely, longitudinal and lateral pendulum modes, characterize the low-speed ($0 \le V \le 12$ m s^{-1}) dynamics of the UAV and that, in the same regime, the plant eigenstructure presents moderate variations for all of the parameters but the coefficient of the imaginary part of the longitudinal pendulum mode. Minor variations affect the frequency of the lateral pendulum mode at low speed. More severe changes occur at higher speed where the same dynamics degenerate into exponentially unstable modes at $V = 13$ and 27 m s^{-1} respectively for the longitudinal and lateral phugoid, and the time constant of the longitudinal mode increases with velocity up to the value of 12 rad s^{-1} at $V = 30$ m s^{-1}.

After linearization, the eight-state rigid-body dynamics of the nominal plant $\boldsymbol{G}_0$ used for control synthesis is written as

$$\dot{\boldsymbol{x}} = \boldsymbol{A}\boldsymbol{x} + \boldsymbol{B}\boldsymbol{a} \tag{1}$$

where $\boldsymbol{x} = (u, v, w, \phi, \theta, p, q, r)^T \in \mathcal{R}^8$ is the state vector and $\boldsymbol{a} \in \mathcal{R}^6$ is the vector of servo angular displacements.

As illustrated in Ref. 2, rotor-blade pitch angles are controlled by two mechanically independent swashplate assemblies, each actuated by a set of three dual rotary servomotors through control rods and linkages. Blade-pitch deflection is nonlinear with servo rotation in a wide region of the vehicle operating range.

The servos accept pulse-width-modulation signals as reference input and are modeled by second-order dynamics with natural frequency $\omega_n = 12.6$ rad s^{-1}, damping coefficient $\zeta = 0.85$, and a constant delay of 0.04 s caused by the pulse-width comparator circuit. The control system generates the pseudocontrol vector $\boldsymbol{u} = (\delta_C, \delta_B, \delta_A, \delta_P)^T \in \mathcal{R}^4$, the elements of which correspond to pilot commands in traditional FCS of helicopters, namely, collective, longitudinal, lateral cyclic, and directional input, respectively. To retain the physical meaning of controller output signals as effectors for altitude, pitch, roll and yaw axes, the six actuator commands $\boldsymbol{u}_s$ are determined from a linear approximation of the relation between blade pitch $\boldsymbol{\Theta}$ and servo position $\boldsymbol{a}$ at hovering, in the form

$$\boldsymbol{\Theta} = \boldsymbol{\Theta}_H + \boldsymbol{E}\boldsymbol{a}$$

where $\boldsymbol{\Theta} = [\boldsymbol{\vartheta}_U, \boldsymbol{\vartheta}_L]^T$ and $\boldsymbol{\vartheta} = (\vartheta_0, \vartheta_1, \vartheta_2)^T$, the blade-root pitch angle being $\vartheta = \vartheta_0 + \vartheta_1 \sin\psi_b + \vartheta_2 \cos\psi_b$. Next, $\boldsymbol{E} = (\partial\boldsymbol{\Theta}/\partial\boldsymbol{a})_H$ while the vector $\boldsymbol{\Theta}_H = (\vartheta_{0_{H_U}}, 0, 0, \vartheta_{0_{H_L}}, 0, 0)^T$ gives the blade pitch at hovering. Collective and cyclic pitch signals are translated into blade pitch angles as

$$\boldsymbol{\Theta} = \left(\delta_C + \tfrac{1}{2}\delta_P, \delta_A, \delta_B, \delta_C - \tfrac{1}{2}\delta_P, \delta_A, \delta_B\right)^T$$

Therefore, the static matrix $\boldsymbol{C}$ that transforms the pseudocontrol into $\boldsymbol{u}_s$ is defined as

$$\boldsymbol{u}_s = \boldsymbol{E}^{-1}\begin{bmatrix}\boldsymbol{N}_U \\ \boldsymbol{N}_L\end{bmatrix}\boldsymbol{u} = \boldsymbol{C}\boldsymbol{u}$$

where

$$\boldsymbol{N}_{U;L} = \begin{bmatrix}1 & 0 & 0 & 0.5; -0.5 \\ 0 & 1 & 0 & 0 \\ 0 & 0 & 1 & 0\end{bmatrix}$$

B. Design Process

The full-envelope FCS is based on the design of two robust controllers, each operating in a subset of the UAV flight envelope and capable of retaining adequate stability and performance characteristics in a rather wide range of level flight speed. As a result of the eigenvalue variation vs speed just outlined, the synthesis process is carried out on the nominal models of the UAV obtained from the linearization of the plant dynamics at trim speeds of 9 and 23 m s^{-1}. Low- and high-speed controller requirements are specified as follows:

1) *Stability:* Adequate margins shall be guaranteed for the stability robustness, assessed by μ analysis, against the considered level of unstructured uncertainty. For SISO loops we should have gain margin $\ge$6 dB and phase margin $\ge$40 deg. Stability robustness shall be also checked against unmodeled dynamics at frequency higher than 2 rad s^{-1}.

2) *Bandwidth:* For the gain crossover frequency, the requirement is ω_{gc} between 2 and 4 rad s^{-1} according to the transfer functions specified in the ideal model. High values of ω_{gc} are impractical because of limitation on servo bandwidth as well as to avoid servo rate and/or position saturation for disturbance rejection in the unstable open-loop plant.

3) *Disturbance rejection:* Turbulence input bandwidth was estimated at 0.2 and 0.5 rad s^{-1} at flight speed of 5 and 25 m s^{-1}, respectively. The specified closed-loop bandwidth is expected to guarantee adequate attenuation of this low-frequency disturbance.

4) *Noise rejection:* Measurement noise shall be attenuated by a factor of 0.1 at frequency of 314 rad s^{-1}, that is, rotor rate, and higher.

The design scheme adopted for both controllers $\boldsymbol{K}$ is shown in Fig. 4, where $\boldsymbol{r} = [h, p, q, r]_{\text{com}}$ and $\boldsymbol{n}$ are, respectively, pilot command and sensor noise, $\boldsymbol{y} = [h, p, q, r]$ is the vector of measured outputs, $\bar{\boldsymbol{e}}$ is the error between the ideal response model and closed-loop response, and $\boldsymbol{w}$ is the perturbation vector. Servo dynamics [block $\boldsymbol{S}(s)$ with output $[\boldsymbol{a}, \dot{\boldsymbol{a}}]^T$] add 12 states to the airframe model, whereas the block $\boldsymbol{D}(s)$ accounts for the first-order Padè approximation of the sum of servo delay and a 0.01 s computational delay, which results from the specification of 100-Hz sampling time for the controller implemented on the onboard digital computer.

The control objective is to find a linear, time-invariant, dynamic controller $\boldsymbol{K}(s)$ such that for all perturbations $\boldsymbol{\Delta}_{\text{pert}}$ the closed-loop

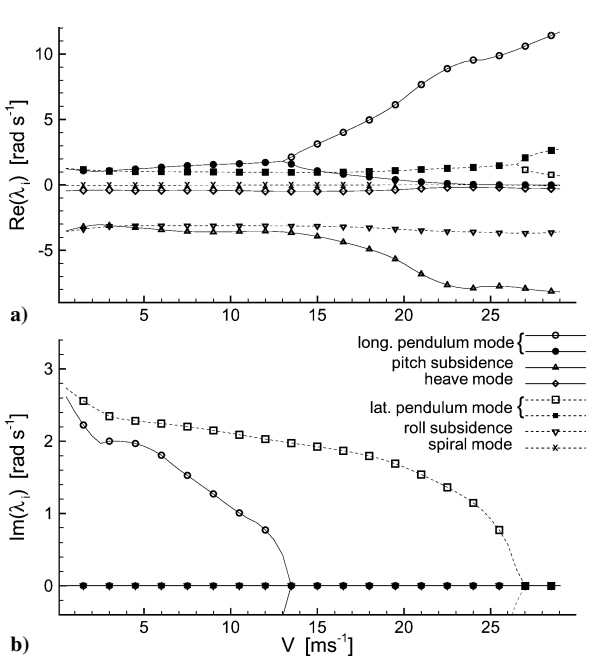

Fig. 3 Root locus as a function of trim speed.

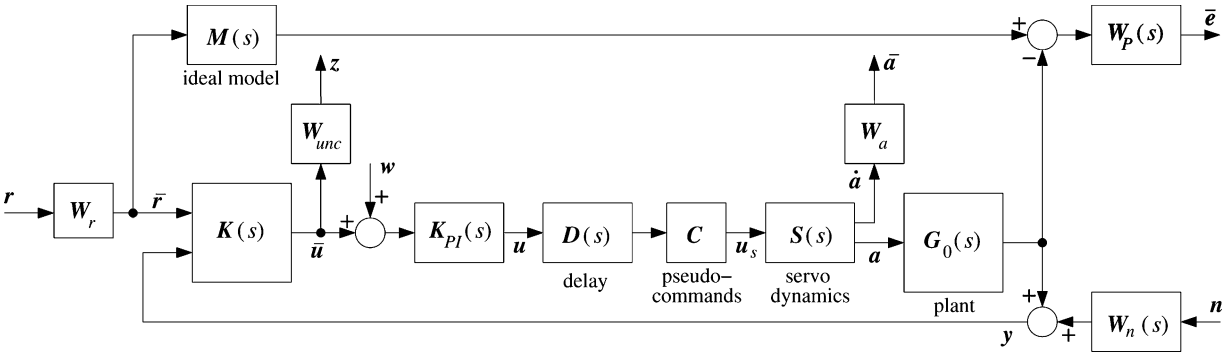

Fig. 4 Two-DOF closed-loop interconnection structure.

system is stable and the condition on performance robustness

$$\|\boldsymbol{T}\|_\infty = \|F_l[F_u(\boldsymbol{P}, \boldsymbol{\Delta}_{\text{pert}}), \boldsymbol{K}]\|_\infty \leq 1 \tag{2}$$

is satisfied, where $\boldsymbol{P}(s)$ is the transfer function of the generalized plant with input $[\boldsymbol{w}, \boldsymbol{r}, \boldsymbol{n}, \bar{\boldsymbol{u}}]$ and output $[\boldsymbol{z}, \bar{\boldsymbol{e}}, \bar{\boldsymbol{a}}, \bar{\boldsymbol{r}}, \boldsymbol{y}]$, given by

$$\boldsymbol{P} = \begin{bmatrix} 0 & 0 & 0 & \boldsymbol{W}_{\text{unc}} \\ -\boldsymbol{W}_P\boldsymbol{G}_0\boldsymbol{S}_p\boldsymbol{C}\boldsymbol{D}\boldsymbol{K}_{\text{PI}} & \boldsymbol{W}_P\boldsymbol{M}\boldsymbol{W}_r & 0 & -\boldsymbol{W}_P\boldsymbol{G}_0\boldsymbol{S}_p\boldsymbol{C}\boldsymbol{D}\boldsymbol{K}_{\text{PI}} \\ \boldsymbol{W}_a\boldsymbol{S}_r\boldsymbol{C}\boldsymbol{D}\boldsymbol{K}_{\text{PI}} & 0 & 0 & \boldsymbol{W}_a\boldsymbol{S}_r\boldsymbol{C}\boldsymbol{D}\boldsymbol{K}_{\text{PI}} \\ 0 & \boldsymbol{W}_r & 0 & 0 \\ \boldsymbol{G}_0\boldsymbol{S}_p\boldsymbol{C}\boldsymbol{D}\boldsymbol{K}_{\text{PI}} & 0 & \boldsymbol{W}_n & \boldsymbol{G}_0\boldsymbol{S}_p\boldsymbol{C}\boldsymbol{D}\boldsymbol{K}_{\text{PI}} \end{bmatrix} \tag{3}$$

where $[\boldsymbol{S}_r, \boldsymbol{S}_p]^T = \boldsymbol{S}$ and

$$\boldsymbol{\Delta}_{\text{pert}} = \text{diag}\left\{\delta_1^C \boldsymbol{I}_{q_1}, \ldots, \delta_n^C \boldsymbol{I}_{q_n}\right\} : \delta_i^C \in C \tag{4}$$

Unstructured multiplicative uncertainty on the four input channels is used to account for model variations as a function of flight speed and poorly identified aerodynamic parameters. In particular, a suitable set of uncertain systems $\boldsymbol{L}$ is given by

$$\boldsymbol{L} = \{\boldsymbol{G}(s) : \boldsymbol{G}(s) = \boldsymbol{G}_0(s)[\boldsymbol{I} + \boldsymbol{\Delta}(s)] \qquad \boldsymbol{\Delta} \in C, \|\boldsymbol{\Delta}\| \leq 1\} \tag{5}$$

where $\boldsymbol{G}$ is the uncertain plant, $\boldsymbol{G}_0$ is the nominal plant and the bounded uncertainty $\boldsymbol{\Delta}$, defined by

$$\boldsymbol{\Delta} = [\boldsymbol{G}(s) - \boldsymbol{G}_0(s)]\boldsymbol{G}_0(s)^{-1} \tag{6}$$

is expressed as

$$\boldsymbol{\Delta}(s) = \boldsymbol{W}_{\text{unc}}\bar{\boldsymbol{\Delta}}(s) \tag{7}$$

where $\bar{\boldsymbol{\Delta}}(s)$ is an unknown stable transfer function, such that $\|\bar{\boldsymbol{\Delta}}\|_\infty \leq 1$.

The PI element is used, as usual, to increase low-frequency gain of the singular values of the unaugmented plant and reduce the rolloff at gain crossover. It also provides an attitude-hold response type, so as to keep constant attitude with zero operator commands on angular rates. The expression for the PI filter is

$$\boldsymbol{K}_{\text{PI}} = [(s + 10)/s]\boldsymbol{I}_{4\times 4} \tag{8}$$

where the unit proportional gain determines crossover frequency of the open-loop plant at 4 and 12 rad s^{-1} for the design points at 9 and 23 m s^{-1}, respectively.

The ideal model $\boldsymbol{M}(s)$ decouples the four input channels and is expressed by the transfer functions

$$\boldsymbol{M} = \text{diag}\{M_1, M_2, M_2, M_3\} \tag{9}$$

where

$$M_1 = \frac{1}{5s+1}, \qquad M_2 = \frac{4(s+1)}{s^2 + 3.6s + 4}, \qquad M_3 = \frac{1}{0.5s+1}$$

This results in a first-order dynamics on the vertical velocity and yaw rate channels (M_1, M_3) with time constants of 5 and 0.5 s, respectively. The response on collective axis is rather slow as expected because $\dot{h}$ is an inertial variable, and a smaller value of the time constant would be unnecessarily demanding for the controller synthesis. As for the pitch and roll channels (M_2), a second-order dynamics with unit static gain was used, which represents a short-period response with $\zeta = 0.9$ and $\omega_n = 2$ rad s^{-1}.

The input weighting function $\boldsymbol{W}_r$ is a constant block intended to scale the plant input, namely, the command signals, to 1. To this end, it is

$$\boldsymbol{W}_r = \text{diag}\{3, \pi/18, \pi/18, \pi/18\} \tag{10}$$

that provides, as nominal conditions, maximum inputs equal to 3 m s^{-1}, and 0.174 rad s^{-1} for the collective and angular rate axes, respectively. Ground operator command signals larger than specified in the preceding weight function produce unwanted coupling of response with a significant degradation of closed-loop system performance.

The performance weighting functions $\boldsymbol{W}_P(s)$, used to weight the error between the pilot commanded rate and that of the actual plant response, are represented by low-pass filters so as to accurately track the ideal model at low frequency. The transfer functions are given by

$$\boldsymbol{W}_P = \text{diag}\left\{W_{P_1}, W_{P_2}, W_{P_3}, W_{P_1}\right\} \tag{11}$$

where it is

$$W_{P_1} = \frac{K_{P_1}(1+s)}{(1+20s)(1+s/40)}, \qquad W_{P_2} = \frac{K_{P_2}}{1+10s}$$

$$W_{P_{P_3}} = \frac{K_{P_3}}{1+10s}$$

The gains used for the low-speed controller are $K_{P_1} = 80$, $K_{P_2} = 190$, and $K_{P_3} = 290$, which specify a maximum tracking error at steady state equal to 0.013 m s^{-1} on the $\dot{h}$ channel and 0.0053, 0.0034, and 0.013 rad s^{-1} on p, q, and r channels, respectively. For the high-speed controller the gains are slightly lower, that is, $K_{P_1} = 70$, $K_{P_2} = 160$, and $K_{P_3} = 260$, resulting in steady-state errors equal to 0.014 m s^{-1} on the $\dot{h}$ channel and 0.0063, 0.0038, and 0.014 rad s^{-1} on p, q, and r channels, respectively.

The weighting functions on control activity $\boldsymbol{W}_a(s)$ are somewhat specific for the present application because of the uncontrollable pole in the origin in the transfer functions $\boldsymbol{a}(s)/\bar{\boldsymbol{u}}(s)$ and $\boldsymbol{a}(s)/\boldsymbol{w}(s)$ (Fig. 4) when the plant is shaped by a PI element and the actuator position is included among the outputs of the interconnection structure. From the physical point of view, the choice of a nonzero static

gain for the ideal (rate) response model on the three angular velocity components, together with a constant weighting function for the input channels $\boldsymbol{W}_r$, requires a nonconstant, steadily increasing control action in case of a step input. Therefore, it is necessary to disregard constraints on maximum actuator angular displacement, and the issue of position saturation is to be addressed by an appropriate definition of the ideal model, the characteristics of which should prevent the controller from achieving maximum servo position. The only limit on control activity that can be considered during the synthesis process is the maximum slew rate of the rotary servos. Therefore, the static weight

$$\boldsymbol{W}_a = (1/1.75)\boldsymbol{I}_{6\times 6} \tag{12}$$

is used to keep the actuator rate below the saturation limit of 1.75 rad s^{-1}.

Next, the weight function $\boldsymbol{W}_n$ represents the noise model for the sensors. Measurement errors ranging from 0.3 to 1.0% of maximum expected value of vertical velocity at low and high frequency were considered, respectively. As for the angular rates, the corresponding levels are 1.6 and 5% of maximum value (nominal). In summary, the weight matrix is

$$\boldsymbol{W}_n = \text{diag}\left\{W_{n_1}, W_{n_2}, W_{n_2}, W_{n_2}\right\} \tag{13}$$

where

$$W_{n_1} = 0.03[(s+1)/(s+3)], \qquad W_{n_2} = 0.00087[(s+1)/(s+3)]$$

After several trials, where the effects of either low-pass and high-pass filters were evaluated, the weighting function of plant uncertainty was set to a constant value[22] as

$$\boldsymbol{W}_{\text{unc}} = 0.2\boldsymbol{I}_{4\times 4} \tag{14}$$

which can be regarded as a quantitative estimation of the performance robustness margins with respect to model uncertainties. The 20% level of uncertainty represents a reasonable tradeoff as larger values determine a higher than unity peak of the structured singular value in robust performance plots, whereas a reduction of the weight degrades the model tracking characteristics of the controlled plant in nonlinear simulation. The multiplicative form of the uncertainty model produces an excessively conservative evaluation of the performance robustness margin.

Control law synthesis is carried out in the framework of the D-K iteration algorithm using the MATLAB® μ-Analysis and Synthesis Toolbox.[23] Controllers with 64 states were obtained, the order of which was reduced to 34 states for the two designs through balanced truncation and optimal Hankel norm approximation.[23]

The μ analysis shows that the low- and high-speed control systems have both robust stability (μ peak values at 0.51 and 0.70, respectively) and performance (μ peak values are 0.90 and 0.85) and that the order reduction has negligible effect on these characteristics.

As a first analysis of control system against frequency-domain specifications, Bode plots of single loops broken at plant input show that gain and phase margins for both the controllers in design conditions are higher, respectively, than 6 dB and 42 deg. Accordingly, the minimum value of the stability margin

$$\epsilon = \max_{\text{stab } K} \|\boldsymbol{n} \to \tilde{\boldsymbol{e}}\|_\infty^{-1}$$

is slightly larger than 0.3, which is considered good for the present application.

Next, Fig. 5 shows singular values of the loop gain for the low (Fig. 5a) and high-speed (Fig. 5b) controllers including the PI element, plotted against stability and performance barriers. Singular values identified by dashed and continuous lines indicate the dominant response associated to r, $\dot{h}$ and p, q inputs. The system is required to have zero steady-state error on yaw rate r and rate-of-climb response $\dot{h}$ (-20 dB/dec barrier at $\omega \le 2$ rad s^{-1}). Note that typical bandwidth requirements (about 4 rad s^{-1}) used for full-scale

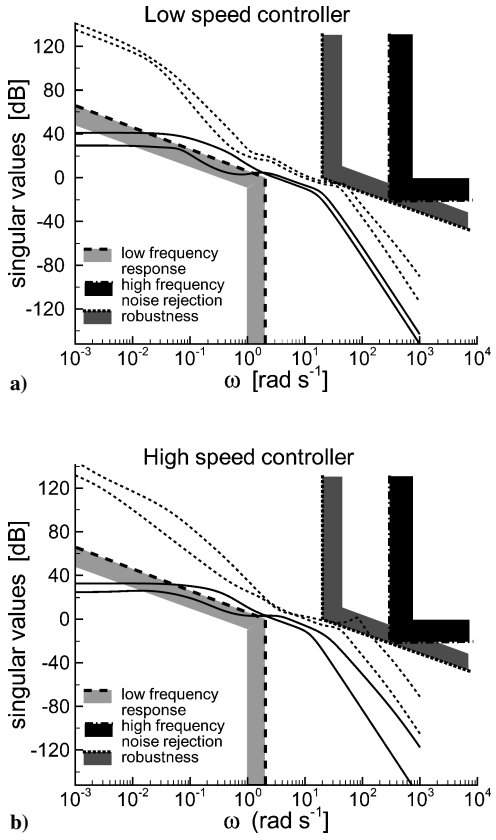

Fig. 5 Singular values of the loop gain of $G_0S_pCDK_{\text{PI}}K$.

helicopters[24] are somewhat relaxed in the present design, as the minimum allowed value for the gain crossover frequency is at 2 rad s^{-1}. As for roll and pitch-rate responses, once low-frequency zeros are cancelled by the PI element, the controller is able to achieve gains higher that 23 dB over the frequency range of interest. Next, consideration of rotor rpm sets the high-frequency barrier for noise rejection of -20 dB at 314 rad s^{-1}. Finally, requirement on stability robustness at high frequency, where we assumed a reasonable model accuracy up to 2 rad s^{-1} with an unbounded growth at 20-dB/decade rate,[25] provides the fourth barrier in the figures. It is apparent that the loop-gain plots meet the specifications in most cases. In the frequency range 30–100 rad s^{-1}, stability robustness against high-frequency model uncertainty is not guaranteed by the high-speed controller.

C. Control Switching

To evaluate the FCS characteristics across the flight envelope, the maximum values of μ for robust stability and performance were plotted as a function of airspeed. The results show that robust stability ($\mu < 1$) is achieved up to 20 m s^{-1} by the low-speed controller $\boldsymbol{K}_{\text{LS}}$ and in the range $2 \le V \le 28$ m s^{-1} by the high-speed controller $\boldsymbol{K}_{\text{HS}}$, whereas the requirement on robust performance is satisfied for $0 \le V \le 19$ and $15 \le V \le 28$ m s^{-1} by, respectively, $\boldsymbol{K}_{\text{LS}}$ and $\boldsymbol{K}_{\text{HS}}$. Accordingly, feasible operating envelopes of $\boldsymbol{K}_{\text{LS}}$ and $\boldsymbol{K}_{\text{HS}}$ were defined, respectively, from hovering to 20 m s^{-1} and from 13 m s^{-1} up to the maximum level speed of 28 m s^{-1}, whereas the threshold velocity, at which the switching logic transfers the control authority from $\boldsymbol{K}_{\text{LS}}$ to $\boldsymbol{K}_{\text{HS}}$ (or vice versa), is placed at $V = 16$ m s^{-1}. A 4 m s^{-1} hysteresis on the switching speed is introduced to avoid the problem of control chatter during transition.

Although the high-gain approach[15] does not completely eliminate the "bump" in the control action when the switching threshold is traversed, this method was selected for the present application because its implementation is more intuitive and does not require any particular property on both the controllers and/or the plant.

The switching control logic is shown in the sketch of Fig. 6a, where the two controllers work in parallel and the output of either

$\boldsymbol{K}_{\mathrm{LS}}$ or $\boldsymbol{K}_{\mathrm{HS}}$ is selected as input to the plant, depending on V. The block $\boldsymbol{K}_{\mathrm{hg}}$ is a constant gain matrix given by $\boldsymbol{K}_{\mathrm{hg}} = 6\,\boldsymbol{I}_{4\times 4}$. According to the high-gain approach,[15] we determined the maximum gain that satisfies classic requirement for stability of the system presented in Fig. 6b, where the output $\boldsymbol{u}_{\mathrm{off}}$ of the offline controller $\boldsymbol{K}$ is requested to track the output $\boldsymbol{u}_{\mathrm{on}}$ of the online controller. The feedback $\boldsymbol{y}$ and the pilot reference signal $\boldsymbol{r}$ are regarded as disturbances. In particular, the value of six for the gain provides closed-loop poles in the left-hand plane and positive gain and phase margins of the open-loop SISO transfer functions $u_{\mathrm{off}_j}/u_{\mathrm{on}_j}$, where the stable and exactly known plant $\boldsymbol{K}$ is equal either to $\boldsymbol{K}_{\mathrm{LS}}$ or $\boldsymbol{K}_{\mathrm{HS}}$.

III. Evaluation of Performance

At this point, controller evaluation is conducted through the analysis of compliance of the closed-loop system with the specifications in ADS-33E for the RCAH response type.[20] As already said in Sec. I, handling-quality requirements taken from ADS-33E specifications were not scaled. The objective is mainly to assess the dynamic characteristics of the vehicle against a reasonable—for the considered application—set of reference guidelines. Then, command response in selected situations is determined by real-time, hardware-in-the-loop (HITL) simulation of the UAV motion.

Table 2 reports the values of bandwidth and phase delay parameters, damping factor and coupling for the controllers. Further results of control system analysis against ADF-33E requirements, in the design conditions, are summarized in Table 3. It is apparent that, although some improvement could be realized in those circumstances in which level 2 response is obtained, standard specifications for military helicopters are fully satisfied for a number of requirements.

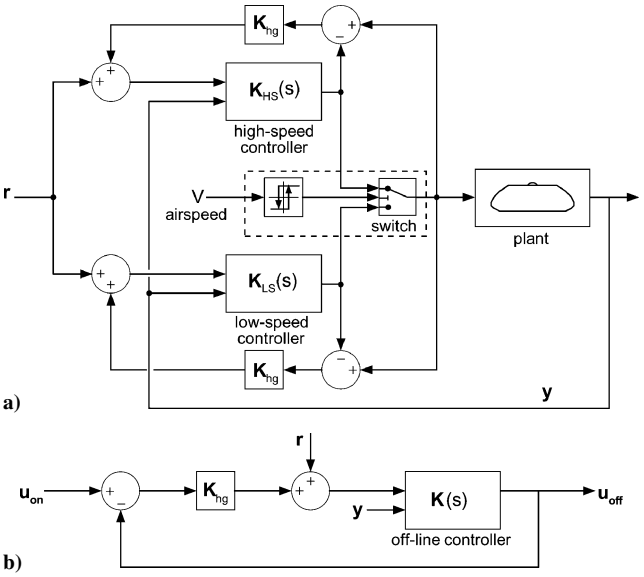

Fig. 6 Sketch of a) control system with switching logic and b) stability analysis for controller conditioning.

FCS analysis is carried out in a HITL simulation facility[21] using dSPACE processor board and related software for the UAV simulation in real time. The system is built around a complete nonlinear model of the vehicle developed in the Mathworks' MATALAB/Simulink software environment. The model features a detailed database for the aerodynamic coefficients of the airframe[1,26] in the full range of variation of angle of attack, inflow velocity, and flight speed. Identified dynamics of servos, sensor noise, and the rpm governor that regulates the throttles of the three engines in order to maintain a constant rotor rate[21] are also incorporated in the simulator. Atmospheric turbulence inputs are computed by a Dryden model with a rather high intensity of 4 m s^{-1} at 100 m altitude.

The control system, including $\boldsymbol{K}_{\mathrm{LS}}(s)$, $\boldsymbol{K}_{\mathrm{HS}}(s)$, and $K_{\mathrm{PI}}(s)$, is discretized using Tusting bilinear transformation at sampling frequency of 100 Hz and implemented into the 266-MHz onboard computer in PC/104 format. Control inputs are generated at the vehicle ground control station that includes the operator console and the graphical user interface (GUI), where flight data and the image of onboard video camera are displayed. Telemetry uplink/downlink between ground station and onboard PC is realized by wireless serial modems communicating at 20-Hz data rate. As a result, the system allows the evaluation in the design process of the relevant effects of telemetry delay and the characteristics of GUI used in the ground station.

Banked turn conditions as a result of roll rate commands are obtained by feeding back to the controller the difference between the actual angular rates and their values for a steady turn. This approach proved to be effective in forward flight, whereas RC response type is retained at very low speed ($V \leq 3$ m s^{-1}). During simulations, the ground operator reported a satisfying level of handling qualities in the full range of forward speed $0 \leq V \leq 29$ m s^{-1} and no difficulty for controlling the vehicle and suppressing disturbance caused by atmospheric gust.

Table 3 Handling-quality evaluation

Requirement	Result
Command tracking	As stated in the specifications, the closed-loop system shows satisfactory tracking capabilities in the low-frequency range
Disturbance rejection	In the low-speed range, 70% of the energy of disturbances entering the system is filtered. The disturbance rejection performance decreases for high speeds, higher than 24 m s^{-1}, providing only a 40% attenuation
Sensor noise attenuation	Less than 1% sensor noise is transmitted to the system output
Attitude quickness	Level 1 is achieved only on the pitch channel, whereas level 2 response is obtained for roll and yaw dynamics
Attitude hold	Attitude-hold response type is obtained

Table 2 Handling-quality parameters for the two controllers

Requirement	Channel	Low-speed controller (9 m s^{-1})	Level	High-speed controller (23 m s^{-1})	Level
Bandwidth and phase delay	ϕ	BW = 1.9 rad s^{-1}, $\tau_p = 0.0032$ s	2	BW = 1.8 rad s^{-1}, $\tau_p = 0.0033$ s	2
	θ	BW = 2.1 rad s^{-1}, $\tau_p = 0.0027$ s	1	BW = 2.2 rad s^{-1}, $\tau_p = 0.0023$ s	1
	ψ	BW = 0.5 rad s^{-1}, $\tau_p = 0.0054$ s	2	BW = 0.5 rad s^{-1}, $\tau_p = 0.0077$ s	2
Damping factor	Pitch	$\zeta = 0.9$	1	$\zeta = 0.9$	1
	Roll	$\zeta = 0.9$	1	$\zeta = 0.9$	1
Coupling	Pitch to roll	$\frac{\Delta\phi_{\max}}{\Delta\theta_{\max}} = 0.24\%$	1	$\frac{\Delta\phi_{\max}}{\Delta\theta_{\max}} = 1.90\%$	1
	Roll to pitch	$\frac{\Delta\theta_{\max}}{\Delta\phi_{\max}} = 1.67\%$	1	$\frac{\Delta\theta_{\max}}{\Delta\phi_{\max}} = 1.67\%$	1

Next, response analysis is carried out by nonpiloted simulations using the same facility, where the required input profiles were implemented in the control station software. Results of step response show that the achieved values of $\dot{h}$, p, q, and r tracks accurately the ideal model with zero steady-state error and the uncoupling between control channels is very satisfactory. For instance, at $V = 9$ m s^{-1} a commanded yaw rate of 10 deg s^{-1} determines peak values of pitch and roll rates less than 0.7 deg s^{-1}, whereas for a 3 m s^{-1} variation of the climb speed the maximum angular rates are less than 0.4 deg s^{-1}.

Figure 7 illustrates the response on the roll (Fig. 7a) and yaw (Fig. 7b) channels to a singlet command. The RCAH response type is evident, and the tracking of the command is satisfactory. Less than 1 s is necessary for achieving the commanded roll rate. The slight overshoot on the roll angle (about 3 deg) with respect to the final attitude is in agreement with the ideal model, the output of which is accurately tracked by the augmented system. The yaw angle response is very smooth and does not present any overshoot, but it is also considerably slower than the response on the roll channel.

The response to a singlet on the pitch control channel, which basically controls airspeed, starting from a hovering condition is reported in Fig. 8. The simulation terminates at $t = 20$ s, when the vehicle achieves a forward speed of 27 m s^{-1} (Fig. 8a). A slight overshoot is present on both pitch attitude and rate (Figs. 8e and 8c). Clearly, the axial symmetry of the configuration together with the same transfer functions in the ideal model produce quite similar response characteristics about the roll (Fig. 7a) and pitch axes. The threshold velocity is acquired at $t = 10.4$ s, and the effect of control switching is visible on the control activity as shown in Fig. 8b ($10.3 \leq t \leq 11.0$ s), where the angular position of the upper rotor servos is plotted, although the q response is reasonably smooth (Fig. 8c). Control axis coupling is very low as roll and yaw rates (Fig. 8c) together with heave velocity remain negligibly small for the whole duration of the maneuver and in spite of switching and the significant variation of plant parameters in the full airspeed range of the UAV.

Next, Fig. 9 shows the response to doublets on pitch ($t = 2.7$ s) and roll ($t = 9$) producing an airspeed variation from 10 to 21 m s^{-1}

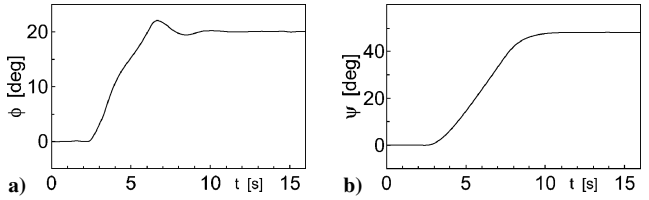

Fig. 7 Singlet response of attitude angles: a) roll axis (5 deg s^{-1} for 4 s) and b) yaw axis (10 deg s^{-1} for 5 s).

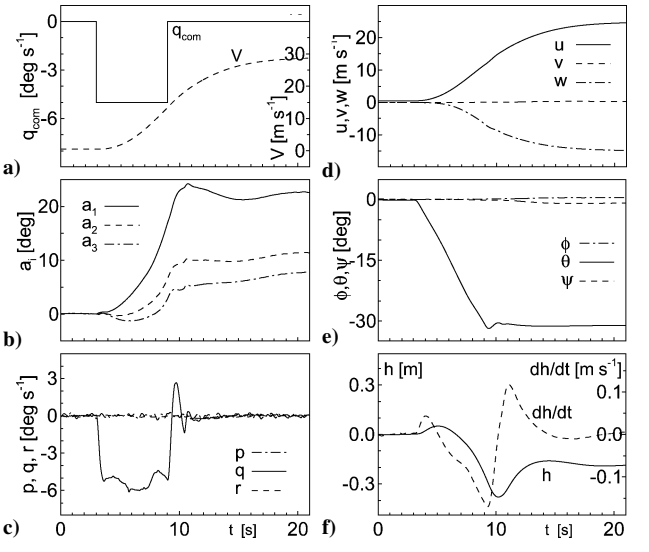

Fig. 8 Acceleration from hovering to high speed.

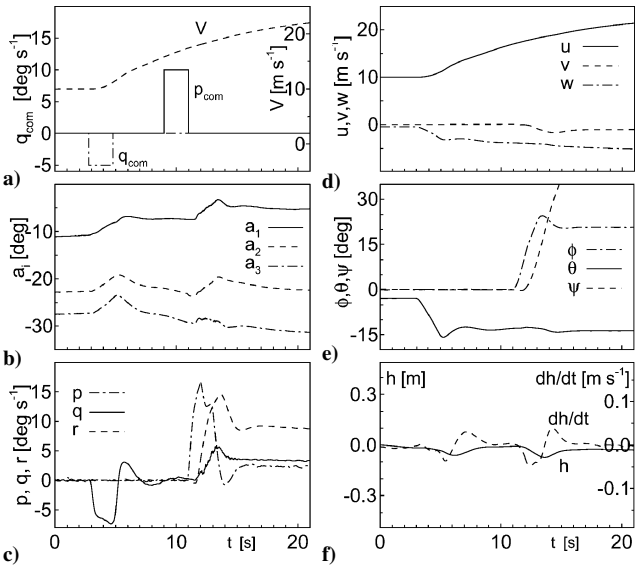

Fig. 9 Acceleration and entrance in a steady turn.

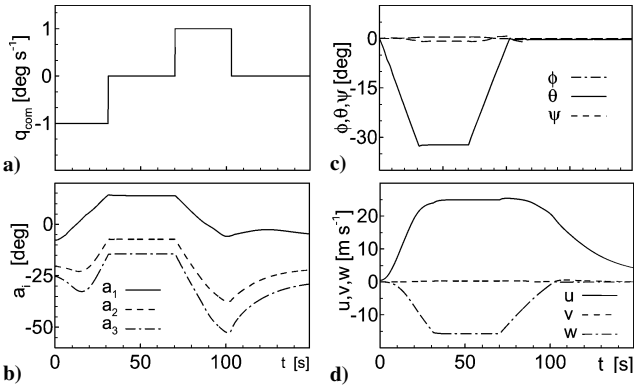

Fig. 10 Effect of c.g. displacement from the nominal position.

(Fig. 9a) and the entrance in a turn at $\phi = 20$ deg (Fig. 9e). In spite of the two-axis command input, a steady value of the roll angle is precisely achieved with a limited overshoot, altitude variation is negligible (Fig. 9f), and the lateral component of velocity is small ($|v| < 1$ m s^{-1} in Fig. 9d), which is relevant considering the very low level of directional stability of the axisymmetric vehicle. Note also that servo angular displacement is moderate (± 5 deg) for the whole duration of maneuver.

Robust behavior of the control system is also tested under external disturbances and uncertainties of system parameters. At airspeed $V = 16$ m s^{-1}, attitude response to a simultaneous gust disturbance on all three axes of the inertial system appears stable even though damping is light in the roll axis. As expected, Euler angles present a slow drift form the initial value because of the single-loop controller structure.

Finally, model uncertainty is introduced by simulating longitudinal ($\Delta x = \pm 0.15$ m) and lateral ($\Delta y = \pm 0.2$ m) offsets of the c.g. with respect to the nominal position on the axis of symmetry of the vehicle. In all of the considered cases, in spite of a significant variation of inertia matrix and trim conditions with respect to the design point, the stability of the augmented vehicle is not degraded in the reference flight condition, and, moreover, performances are only marginally affected. As expected, the worst case is the backward displacement of the c.g., and, in this respect, Fig. 10 shows the simulation of a doublet on the pitch channel that, from hovering, causes the flight speed to increase up to 25 m s^{-1} and then to drop back at about 3 m s^{-1}. The c.g. has a -0.15-m (backward) offset (equal to 30% of the rotor radius) with respect to its nominal position on the symmetry axis of the vehicle. Plots of body axis velocity components, attitude angles, and angular rates show that response is still

satisfying even during the controller transition where the amplitude of Euler angle perturbation is hardly visible. In the same situation, that is, backward c.g. position, some degradation was observed in banked turns performance. Lateral c.g. displacement affects performance to a lower extent than in the previous case, and, in particular, vehicle behavior in banked turns is only marginally affected.

IV. Conclusions

The full-envelope flight control system of a novel shrouded-fan VTOL UAV was designed using the structured-singular-value methodology. Two multivariable controllers were synthesized, for the low- and high-speed operating envelopes, having the same two-DOF structure and a four-axis ideal model where angular rates and vertical velocity are the ground pilot commands. A simple technique is adopted to realize smooth transitions of plant input during switching between controllers at the threshold speed.

RCAH response characteristics are obtained using a single-loop design, where a proportional-plus-integral element is incorporated in the controller structure to avoid such issues as bandwidth reduction and outer-loop adaption caused by attitude tracking performance degradation in off-design conditions, which are frequently encountered in two-loop control structures. By using this approach, the issue of position saturation of servos is not directly addressed in the controller design phase, whereas computer simulation of the closed-loop system showed that, by an adequate selection of ideal model and weight function on control activity, both actuator rate and position requirements can be satisfied.

Each controller was evaluated against ADS-33E handling-quality specifications and produces level 1 performance in most requirement. Level 2 performance on bandwidth and phase delay of roll and pitch channels is not considered critical for the present application. The FCS demonstrated good levels of handling qualities by real-time, hardware-in-the-loop simulation testing. Disturbance rejection and robust performance in off-design conditions, that is, in the full range of airspeed and for a relevant offset of c.g. location with respect to design conditions is also at acceptable levels.

Acknowledgment

This work was supported by the Italian Ministry of University and Scientific Research.

References

[1]Avanzini, G., D'Angelo, S., and de Matteis, G., "Performance and Stability of Ducted-Fan Uninhabited Aerial Vehicle Model," *Journal of Aircraft*, Vol. 40, No. 1, 2003, pp. 86–93.

[2]Avanzini, G., D'Angelo, S., and de Matteis, G., "Design and Development of a Vertical Take-off and Landing Uninhabited Aerial Vehicle," *Journal of Aerospace Engineering*, Vol. 217, No. 4, 2003, pp. 169–178.

[3]Walsh, D., and Cycon, J. P., "The Sikorsky Cypher UAV: A Multi-Purpose Platform with Demonstrated Mission Flexibility," *Proceedings of the American Helicopter Society 54th Annual Forum*, American Helicopter Society, Alexandria, VA, 1998, pp. 1410–1418.

[4]Lipera, L., Colbourne, J., Tischler, M., Mansur, M., Rotkowitz, M., and Patangui, P., "The Micro Craft iSTAR Micro Air Vehicle: Control System Design and Testing," *Proceedings of the American Helicopter Society 57th Annual Forum*, American Helicopter Society, Alexandria, VA, 2001, pp. 1998–2008.

[5]Calise, A. J., Johnson, E. N., Johnson, M. D., and Corban, E. J., "Applications of Adaptive Neural-Network Control to Unmanned Aerial Vehicles," *AIAA/ICAS International Air and Space Symposium and Exposition: The Next 100 Years*, 2003, URL: http://www.ae.gatech.edu/labs/controls/papers/Year/2003.complete.html [cited 5 Nov. 2005].

[6]Shim, H., "Hierarchical Flight Control System Synthesis for Rotorcraft-Based Unmanned Aerial Vehicles," Ph.D. Dissertation, Univ. of California, Berkeley, CA, 2000.

[7]La Civita, M., Papageorgiou, G., Messner, W. C., and Kanade, T., "Design and Flight Testing of a High-Bandwidth H_∞ Controller for a Robotic Helicopter," AIAA Paper 2002-4836, Aug. 2002.

[8]Corban, E. J., Calise, A. J., Prasad, J. V. R., Hur, J., and Kim, N., "Flight Evaluation of Adaptive High-Bandwidth Control Methods for Unmanned Helicopters," AIAA Paper 2002-4441, Aug. 2002.

[9]Mettler, B., *Identification Modeling and Characteristics of Miniature Rotorcraft*, Kluwer Academic, Boston, 2003, Chap. 5.

[10]Mettler, B., Dever, C., and Feron, E., "Scaling Effects and Dynamic Characteristics of Miniature Rotorcraft," *Journal of Guidance, Control, and Dynamics*, Vol. 27, No. 3, 2004, pp. 466–478.

[11]Hess, R. A., and Ussery, T. M., "Sliding Mode Techniques Applied to the Control of a Micro-Air Vehicle," AIAA Paper 2003-5408, Aug. 2003.

[12]Packard, A., and Doyle, J. C., "The Complex Structured Singular Value," *Automatica*, Vol. 29, No. 1, 1993, pp. 71–109.

[13]Shim, H., Koo, T. J., Hoffmann, F., and Sastry, S., "A Comprehensive Study of Control Design for an Autonomous Helicopter," *37th IEEE Conference on Decision and Control*, Vol. 4, Inst. of Electrical and Electronics Engineers, New York, 1998, pp. 3653–3658.

[14]McFarlane, D., and Glover, K., "A Loop Shaping Design Procedure Using H_∞ Synthesis," *IEEE Transactions on Automatic Control*, Vol. 37, No. 6, 1992, pp. 759–769.

[15]Hyde, R. A., *H_∞ Aerospace Control Design. A VSTOL Flight Application*, Springer-Verlag, London, 1995, Chap. 5.

[16]Avanzini, G., de Matteis, G., and Fresta, F., "Robust Multivariable Control of a Shrouded-Fan Uninhabited Aerial Vehicle," AIAA Paper 2002-4703, Aug. 2002.

[17]Walker, D. J., and Postlethwaite, I., "Advanced Helicopter Flight Control Using Two-Degree-of-Freedom H_∞ Optimization," *Journal of Guidance, Control, and Dynamics*, Vol. 19, No. 2, 1996, pp. 461–468.

[18]Postlethwaite, I., Smerlas, A., Walker, D. J., Gubbels, A. W., Baillie, S. W., Strange, M. E., and Howitt, J., "H_∞ Control of the NRC Bell 205 Fly-by-Wire Helicopter," *Journal of the American Helicopter Society*, Vol. 44, No. 4, 1999, pp. 276–284.

[19]Chen, M., and Huzmezan, M., "A Simulation Model and H_∞ Loop Shaping Control of a Quad Rotor Unmanned Air Vehicle," *Proceedings of the IASTED International Conference on Modelling, Simulation, and Optimization*, edited by M. H. Hamza, ACTA Press, Calgary, AB Canada, 2003, pp. 320–325.

[20]"Aeronautical Design Standard Performance Specifications, Handling Qualities Requirements for Military Rotorcraft," U.S. Army, Aviation and Missile Command, ADS-33E, Redstone Arsenal, AL, March 2000.

[21]Avanzini, G., D'Angelo, S., and de Matteis, G., "Modelling and Simulation of a Shrouded-Fan UAV for Environmental Monitoring," AIAA Paper 2002-3464, May 2002.

[22]Rozak, J. N., "Impact of Robust Control on Handling Qualities and Fatigue Damage of Rotorcraft," Ph.D. Dissertation, Dept. of Mechanical Engineering, Pennsylvania State Univ., University Park, PA, May 1995.

[23]Balas, G. J., Doyle, J., Glover, K., Packard, A., and Smith, R., *μ-Analysis and Synthesis Toolbox*, MUSYN, Inc., and Mathworks, Inc., Minneapolis, MN, 1995.

[24]Low, E., and Garrard, W. L., "Design of Flight Control Systems to Meet Rotorcraft Handling Qualities Specifications," *Journal of Guidance, Control, and Dynamics*, Vol. 16, No. 1, 1993, pp. 69–78.

[25]Ridgely, D. B., Banda, S. S., McQuade, T. E., and Lynch, P. J., "Linear-Quadratic-Gaussian with Loop-Transfer-Recovery Methodology for an Unmanned Aircraft," *Journal of Guidance, Control, and Dynamics*, Vol. 10, No. 1, 1987, pp. 82–89.

[26]de Divitiis, N., "Aerodynamic Modeling and Performance Analysis of a Shrouded Fan Unmanned Aerial Vehicle," International Council of the Aeronautical Sciences, Paper 256, Sept. 2002.